Exp Astron (2015) 40:45–60
DOI 10.1007/s10686-014-9378-1

ORIGINAL ARTICLE

The atmospheric monitoring system of the JEM-EUSO instrument

The JEM-EUSO collaboration

Received: 5 November 2013 / Accepted: 4 March 2014 / Published online: 23 July 2014

Abstract The JEM-EUSO telescope will observe Ultra-High Energy Cosmic Rays (UHECRs) from space, detecting the UV Fluorescence Light produced by Extensive Air Showers (EAS) induced by the interaction of the cosmic rays with the earth's atmosphere. The capability to reconstruct the properties of the primary cosmic ray depends on the accurate measurement of the atmospheric conditions in the region of EAS development. The Atmospheric Monitoring (AM) system of JEM-EUSO will host a LIDAR, operating in the UV band, and an Infrared camera to monitor the cloud cover in the JEM-EUSO Field of View, in order to be sensitive to clouds with an optical depth $\tau \geq 0.15$ and to measure the cloud top altitude with an accuracy of 500 m and an altitude resolution of 500 m.

The JEM-EUSO Collaboration for the full author list see the last page of this article.

S. Toscano (✉)
ISDC Data Centre for Astrophysics, Versoix, Switzerland
e-mail: Simona.Toscano@unige.ch

J. A. Morales de los Ríos · M. D. Rodríguez Frías
SPace & AStroparticle (SPAS) Group, UAH, Madrid, Spain

J. A. Morales de los Ríos
e-mail: josealberto.morales@uah.es

M. D. Rodríguez Frías
e-mail: dolores.frias@uah.es

A. Neronov
ISDC Data Centre for Astrophysics, Versoix, Switzerland
e-mail: Andrii.Neronov@unige.ch

S. Wada
RIKEN Advanced Science Institute, Tokyo, Japan
e-mail: swada@riken.jp

Keywords Ultra high energy cosmic rays · Atmospheric monitoring · IR camera · LIDAR

1 Introduction

JEM-EUSO (the Extreme Universe Space Observatory on-board the Japanese Experiment Module) on the International Space Station (ISS) is a new space mission which aims to discover the origin of the Ultra High Energy Cosmic Rays (UHECRs) with energies above $\sim 5 \times 10^{19}$ eV [1, 2]. Looking downward to the earth's atmosphere the JEM-EUSO telescope will detect, with an unprecedented detection aperture, the fluorescence and Cherenkov UV emission from UHECRs-induced Extensive Air Showers (EAS) penetrating in the atmosphere within its 60° Field of View (FoV).

JEM-EUSO will capture the UV photons from the moving tracks of the EAS and reproduce the calorimetric development of the shower in order to measure the properties of the primary cosmic rays. The amount of both fluorescence and Cherenkov signals reaching JEM-EUSO depends on the extinction and scattering properties of the atmosphere. Extinction leads to an overall reduction of the UV light intensity detectable by the telescope, while scattering properties of the atmosphere at the EAS location determine the amount of Cherenkov light which is re-directed toward the telescope. A correct reconstruction of UHECR energy and of the type of the primary cosmic ray particle requires, therefore, information about absorption and scattering of the UV light.

Also, the presence of clouds and aerosol layers will alter the physical properties of the atmosphere. Uncertainties of extinction and scattering coefficients related to the variable meteorological conditions introduce distortions of the UV signal from EAS leading to systematic errors in the determination of the properties of UHECR from the UV light profiles [3, 4].

The Atmospheric Monitoring (AM) system of JEM-EUSO will provide information on cloud cover and the optical properties of cloud/aerosol layers at the time and location of the EAS. This information will be used in the off-line data analysis to correct the shower profile and to reduce the error in the reconstruction. Since the ISS is moving with a sub-satellite point speed of ~ 7 km/sec and an orbital inclination of 51.6° around the Earth, JEM-EUSO will experience all possible weather conditions. The AM system will continuously monitor the varying atmospheric conditions in the JEM-EUSO FoV during all UHECRs data taking periods.

In this paper we review the set up of the AM system and its performance and we describe the system capabilities in recovering cloud optical depth and shower profile based on simulation studies.

2 Atmospheric monitoring system

The goal of the AM system is to obtain information on the distribution and optical properties of clouds and aerosol layers inside the JEM-EUSO FoV [5, 6]. The basic

requirements on the precision of the measurements of the clouds and aerosol layers characteristics can be obtained from the general requirements on the precision of measurements of the UHECRs properties [7], namely:

R1) reconstruction of the UHECR energy with a precision better than 30 %;
R2) determination of the position of the shower maximum (X_{max}) with a precision better than 120 g/cm^2.

Since the energy of the UHECR is proportional to the overall intensity of the UV emission from the EAS, the uncertainty of the energy measurement (R1) will depend on the uncertainty in the determination of the extinction properties in the atmosphere. To limit the maximum uncertainty of the energy determination to be at most 15 % (so that the error introduced by this uncertainty is sub-dominant) the uncertainty of the extinction profile has to be smaller than 0.15. In this conditions the AM system should be able to distinguish the clouds with $\tau \geq 0.15$. The profile of EAS observed in such a region where clouds with $\tau \geq 0.15$ are detected has to be corrected for the extinction losses in order to be used for the spectrum analysis. For those cases in which the correction cannot be performed, the event will be used only for angular reconstruction.

In addition, the depth of the shower maximum will be affected by the uncertainty in the determination of the location and physical properties of clouds and aerosol layers, in such a way that uncertainties in the determination of both extinction and scattering properties of these features will directly affect the precision of the X_{max} measurement (R2). Imposing a maximum of 60 g/cm^2 as a possible contribution to the uncertainty of the X_{max} measurement leads to the conclusion that a measurement of the cloud top with an accuracy $\Delta H \leq 500$ m is required.

The AM system will include [8]:

1. an Infrared (IR) camera;
2. a LIght Detection And Ranging (LIDAR) device;
3. global atmospheric models generated from the analysis of all available meteorological data by global weather services such as the National Centers for Environmental Predictions (NCEP) (http://www.ncep.noaa.gov/), the Global Modeling and Assimilation Office (GMAO) (http://gmao.gsfc.nasa.gov/) and the European Centre for Medium-Range Weather Forecasts (ECMWF) (http://www.ecmwf.int/).

The principle of the AM system in JEM-EUSO is illustrated in Fig. 1. The JEM-EUSO telescope will observe the EAS development only during nighttime. The IR camera will monitor the entire FoV to detect the presence of clouds and to obtain the cloud cover and cloud top altitude during the observation period of the JEM-EUSO main instrument. To achieve the required precision of measurement of the cloud top altitude, the precision of the temperature measurements by the IR camera has to be $\Delta T = 3$ K. The LIDAR will be shot in several directions around the location of each triggered EAS event and it will measure the optical depth profiles of the atmosphere in these selected directions, with a range resolution of $375/\cos\theta_z$ m, where θ_z is the angle between the direction of the laser beam and the nadir. The power of the laser will be chosen in such a way that the LIDAR will be sensitive to the presence of

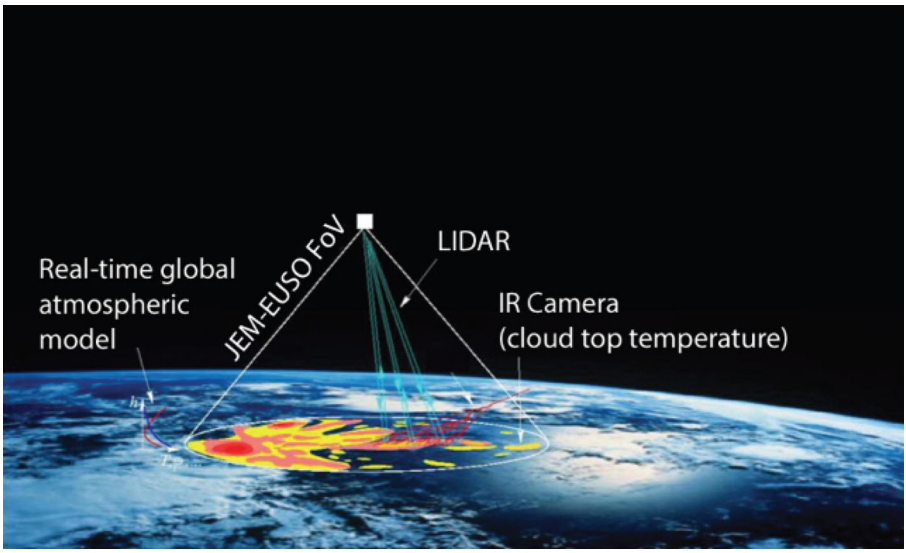

Fig. 1 Sketch of the Atmospheric Monitoring system of JEM-EUSO

cloud/aerosol layers with an optical depth $\tau \geq 0.15$ at 355 nm wavelength. The final goal will be to categorise the scene in three classes: $\tau < 0.15$ (clear atmosphere), $\tau = 0.15 - 1$ (thin clouds) and $\tau > 1$ (thick clouds).

The LIDAR measurements are complementary to the measurements taken by the IR camera. On one hand, the IR camera will provide an overall picture of the optically thick cloud cover in the JEM-EUSO FoV, which is not possible to measure with the LIDAR, since this device can retrieve the optical properties of the atmosphere only for a certain direction. On the other hand, the LIDAR will provide some information about the presence of optically thin clouds and aerosol layers which cannot be identified by the IR camera. In particular, in the case of optically thick low altitude clouds, the detection of the LIDAR backscattered signal from the cloud top layers will be used as an additional information to the IR camera measurement. The timing of the received signal, together with the IR camera detection, will allow for the measurement of the altitude of the cloud with an accuracy of 500 m.

Finally real-time atmospheric profiles from global models will be used as an input for the off-line analysis of LIDAR data, calibration of IR camera and modelling of the EAS development in the atmosphere and its reconstruction.

Statistical studies of clouds and aerosol distribution show that $\sim$ 70 % of the UHECRs events will be affected by the presence of clouds while only $\sim$ 30 % will develop in clear atmosphere conditions [9–11]. The minimal task of the AM system is to provide an efficient quality criterion for the selection of the clear atmosphere or "golden" events (because these are easier to reconstruct). In addition, a step forward will be obtained using the AM system to define a subset of events appearing in cloudy regions but still suitable for analysis, such as an EAS hitting the top of a low-altitude optically thick cloud. Measurements done with LIDAR and IR camera will be used

to correct the cloud affected EAS profiles which could be finally retained for further analysis.

3 Infrared camera

The IR camera of JEM-EUSO is an infrared imaging system for detecting the presence of clouds in the FoV of the JEM-EUSO main telescope and for obtaining the cloud cover and cloud top altitude during the observation period of the JEM-EUSO main instrument. Its full design, prototyping, space qualified construction, assembly, verification and integration is under the responsibility of the Spanish Consortium involved in JEM-EUSO. Since measurements will be performed at night, they will be based on cloud IR emission. The observed radiation is basically related to the target temperature and emissivity and can be used to infer an estimate of the clouds top altitude. The IR camera onboard JEM-EUSO will consist of refractive optics made of germanium and an uncooled μbolometer array detector [12]. The FoV of the IR camera will totally match the FoV of the main JEM-EUSO telescope. The angular resolution, corresponding to one pixel, is about 0.1°. A temperature-controlled shutter in the camera and two blackbodies form part of the calibration unit dedicated to manage and control the camera calibration operation. This unit guarantees a reference internal temperature and it is used to calibrate the background noise and gains of the detector to achieve an absolute temperature accuracy of $\sim$ 3 K. Though the IR camera takes images continuously, the transfer of the images takes place every $\sim$17 s, in which the ISS moves $\sim$1/4 of the FoV of the JEM-EUSO telescope.

To accomplish the mission and scientific requirements for the IR camera, a System Preliminary Design (SPD) of a prototype is under development by the Spanish

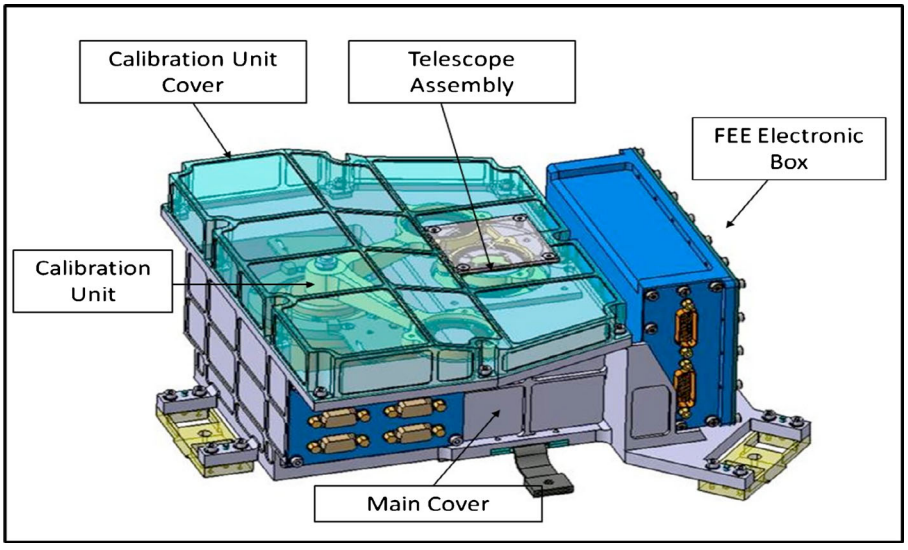

Fig. 2 Illustrative figure of the IR Camera design

Consortium [13]. This design is based on an uncooled microbolometer which will measure the infrared emission from the atmosphere, in two windows within the 10 to 12.5 μm wavelength bands, matching the Field of View and spatial resolution of the main Telescope. A schematic illustration of the camera hardware being designed can be seen in Fig. 2. A detailed status of the IR camera design will be presented in "The Infrared Camera on-board JEM-EUSO Space Observatory" in this edition [14].

4 LIDAR

The task of the LIDAR is to provide measurements of the scattering and extinction properties of the atmosphere in the region of the EAS development and between the EAS and the JEM-EUSO telescope.

4.1 The instrument

The LIDAR is composed of a transmission and receiving system. The transmission system comprises a Nd:YAG laser and a pointing mechanism to steer the laser beam in the direction of triggered EAS events.

The specifications of the laser unit of the LIDAR system are similar to the laser ranging devices on board of several satellites for atmospheric sounding purposes such as the NASA satellite CALIPSO (http://www-calipso.larc.nasa.gov/). The main difference from the previous space-based lasers is that the operational wavelength (λ = 355 nm) will be the third harmonic (rather than the first, at 1064 nm, or the second, at 532 nm, as in existing systems) of the Nd:YAG laser which is conventionally achieved with the frequency-tripling crystal placed inside the laser beam. LIDAR measurements should probe the atmosphere at the location of each triggered EAS event. To perform such measurements the laser beam has to be pointed in the direction of the EAS events. This will be achieved using a steering mirror system with two angular degrees of freedom and a maximal tilting angle of $\pm 15°$, needed to point the laser beam in any direction within the JEM-EUSO FoV.

The timing properties of the LIDAR backscattered signal are similar to the timing properties of the EAS events, which allows to use the main JEM-EUSO telescope as a receiver for the LIDAR signal. Any Multi-Anode Photo-Multiplier Tube (MAPMT) [15] in the focal surface of the JEM-EUSO telescope could serve as the LIDAR signal detector; while a special LIDAR trigger is foreseen in the focal surface electronics of the JEM-EUSO detector [16]. The EAS trigger generated in a given Photo Detector Module (PDM) [17] will also generate a command to re-point and shoot the laser beam in the direction of the triggered EAS. After a certain time delay, the pixels of the PDM will switch in the mode of reception to detect the LIDAR signal.

A summary of the specifications for the entire system is reported in Table 1.

Measurements of the laser backscatter signal with a time resolution of 2.5 μs (representing the duration of the time unit, named Gate Time Unit or GTU, of the focal surface detector) will provide a ranging resolution of 375 m in the nadir direction. The energy of the laser pulse will be chosen so that the backscattered signal will have

Table 1 Specification for the JEM-EUSO LIDAR

Parameter	Specification
Wavelength	355 nm
Repetition rate	1 Hz
Pulse width	15 ns
Pulse energy	20 mJ/pulse
Beam divergence	0.2 mrad
Receiver	JEM-EUSO telescope
Detector	MAPMT (JEM-EUSO)
Range resolution (nadir)	375 m
Steering of output beam	$\pm 30°$ from nadir
Mass	14 kg
Dimension	$450 \times 350 \times 250$ mm
Power	< 20 W

enough statistics for the detection and measurement of the optical depth of optically thin clouds with $\tau \geq 0.15$ at large off-axis angles.

To study the performance of the LIDAR, a simulation of this device has been implemented into the ESAF Simulation Framework [18] used for the JEM-EUSO mission. In the simulation a given number of LIDAR photons are generated accordingly with the laser energy, $N_\gamma = E_{laser}/(hc/\lambda)$, and propagated through the atmosphere adapting the algorithm used for the light propagation for the case of air showers [19]. Clouds of different altitude and optical depth have been simulated within the ESAF framework . Since the LIDAR will be used to shoot the shower in several directions, the signal has been simulated also varying the nadir angle θ_z with respect to the nadir. Results of these simulations are presented in Fig. 3. In the left panel of the figure the minimum energy of the laser pulse (shot in the nadir position) needed to detect clouds of different physical properties is given as a function of the cloud top altitude. The three lines represent the fits to simulated data for three different optical depths. The requirement for the LIDAR system, represented with a solid line, is the capability to detect features with $\tau \geq 0.15$. Simulated data (solid points) are displayed only for the case $\tau = 0.15$ to simplify the plot. The right panel of the same figure shows the minimum energy of the laser pulse needed to detect cloud with $\tau = 0.15$ as a function of the nadir angle. Results are shown for an altitude of 5 and 10 km. When the laser beam is inclined the energy needed to detect the cloud is higher with respect to the case in which the laser is shot in nadir since the laser beam has to cover a longer path in the atmosphere.

4.2 Data analysis

The LIDAR simulation chain has been used to study the features of the backscattered signal and to reproduce a real-case observation in which the EAS profile shows observable deviations from the “clear atmosphere case” and needs to be corrected.

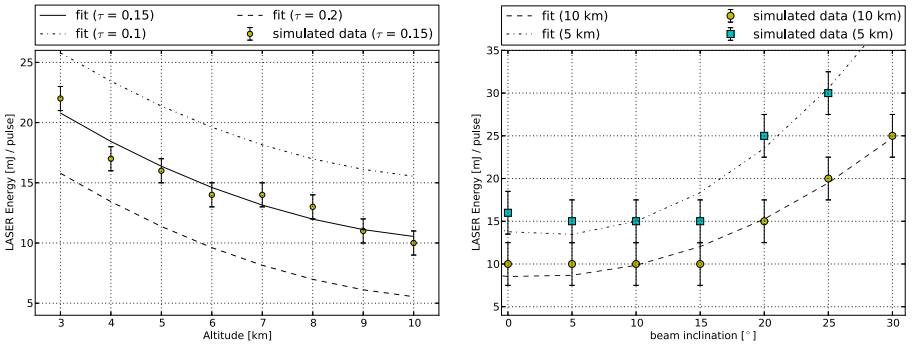

Fig. 3 *Left panel* Laser energy as a function of the cloud top altitude. The plot represents the minimum energy per pulse needed by the LIDAR in order to detect clouds at several altitudes. The points represent the simulated data for an optical depth of the cloud $\tau = 0.15$ (requirement for the LIDAR of the AM system) and the line is a polynomial fit to the data. The polynomial fits for optical depth $\tau = 0.1$ and $\tau = 0.2$ are plotted for comparison. *Right panel* Laser energy as a function of the beam direction with respect to the nadir. The plot represents the minimum energy per pulse needed to detect clouds (with $\tau = 0.15$) at 5 km (*squares*) and 10 km (*circles*) for different beam directions with respect to the nadir

For this purpose, a UHE proton with E = 10^{20} eV and $\theta = 60°$ has been simulated in both clear atmosphere and cloudy conditions. The profile of the detected photo-electron signal as a function of GTU is shown in Fig. 4. The blue circles represent the shower time profile in clear atmosphere conditions and it is characterized by the presence of a feature at ~ 60 GTU, the "ground mark", due to Cherenkov photons hitting the ground and reflected back to the JEM-EUSO focal surface. The second profile in red represents the shower crossing an optically thick cloud ($\tau = 1$) located at an altitude of 7 km. The cloud mark (green band), generated by photons reflected by the cloud top layers, is visible this time, while the Cherenkov mark from the ground is strongly suppressed.

As already discussed in Section 2, one of the main goals of the AM system is to provide information of atmospheric properties to reconstruct EAS parameters from the cloud affected profiles. It will be possible to reconstruct the undisturbed profile (as it would be in clear atmosphere conditions) from the observed one by applying corrections based on the LIDAR measurements of the cloud optical depth.

Examples of the simulated laser backscatter signal as it would appear in the JEM-EUSO detector are shown in Fig. 5. The top panel shows the signal in case of clear atmosphere (blue circles) and in presence of the cloud (red triangles) as a function of the time after shooting the laser and the altitude. The presence of a cloud at $\sim$7 km will be clearly detected by the LIDAR as an increase of the backscattered signal coming from that region. The bottom panel shows the so-called LIDAR Scattering Ratio (SR), the ratio between the backscattered signal detected in the real condition and a reference profile which represents the backscattered signal in clear atmosphere. In case of presence of clouds, the suppression of the backscattered signal is related to the cloud optical depth (τ), as:

$$\tau = -\frac{1}{2}\ln(SR). \tag{1}$$

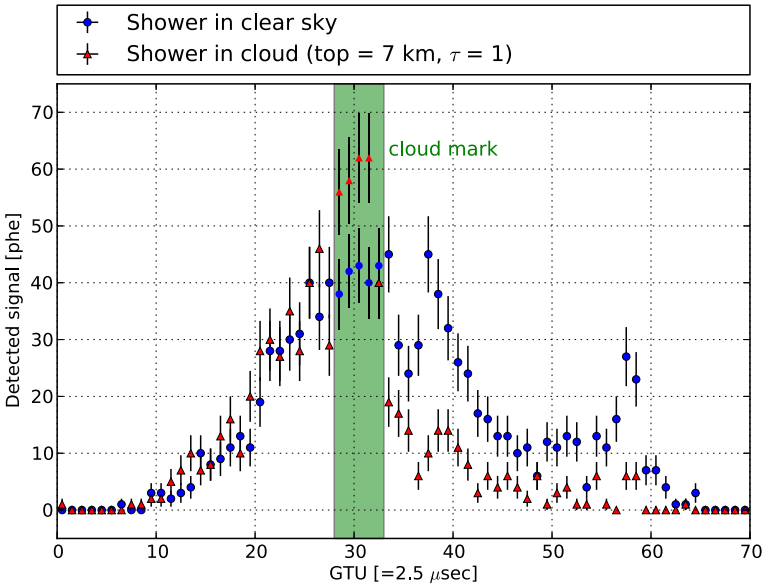

Fig. 4 Time profile of 10^{20} eV EAS in clear atmosphere conditions (*blue circles*) and in the presence of a cloud with $\tau = 1$ and top = 7 km (*red triangles*). The "ground mark", due to Cherenkov photons reflected by the ground, is clearly visible in the clear atmosphere profile, while it is suppressed in the presence of the optically thick cloud. The profile in presence of a cloud is characterized instead by the cloud mark (*green band*), generated by photons reflected toward the detector from the top layers of the cloud

Fitting the SR in the region below the cloud allows the optical depth of the cloud to be determined, simply using (1). For the case reported in Fig. 5, an optical depth $\tau = 1.05 \pm 0.05$ has been retrieved from this procedure ($\tau = 1$ was assumed in the simulation). The fitting procedure has also been applied to the region above the cloud and a value of SR $\simeq 1$ has been measured as expected.

Once the cloud is detected and its optical depth determined, the EAS profile can be corrected using the following equation:

$$Signal_{cloud} = Signal_{clear} \cdot \exp(-\tau). \tag{2}$$

The result of this correction is illustrated in Fig. 6 where the reconstructed profile is shown. The statistical uncertainties are calculated by propagating the uncertainty of the optical depth measurement. Lack of information on the optical depth profile inside the cloud does not allow for a correct reconstruction of the shower profile in that region. It is worth noticing that the ground mark is almost entirely recovered by this analysis procedure.

The systematic uncertainties have not been quantified at this stage of the analysis and they are not included in the measurement. The sources of systematic uncertainties for atmospheric measurements are of different nature. Atmospheric profiles are used to calculate the amount of light generated by the passage of the air shower. The

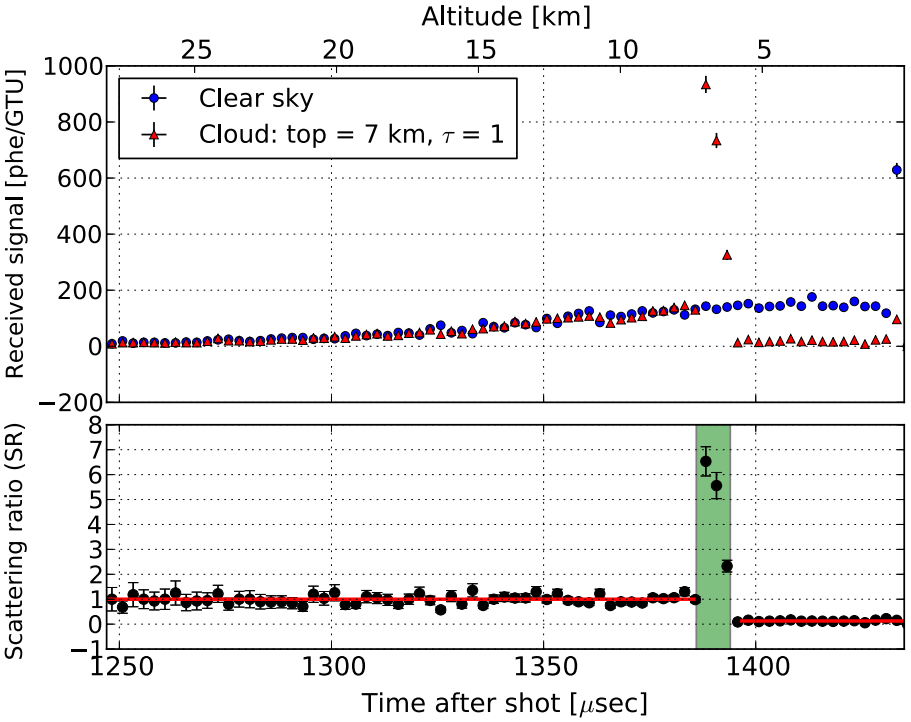

Fig. 5 *Top* LIDAR backscattered signal in clear atmosphere (*blue*) and in the presence of a cloud (*red*) as a function of time. *Bottom* Scattering ratio (SR) for the case of LIDAR shooting an optically thick ($\tau = 1$) cloud located at an altitude of 7 km. The cloud mark region is highlighted with a green box. A fit of the SR is shown as a red line. A value of SR $\simeq 1$ is obtained for the region above the cloud, indicating no difference between the clear atmosphere and the observed one. On the other hand, fitting the SR in the region below cloud it allows the retrieval of the cloud optical depth

use of Global Atmospheric Models (see next section) for the calculation will allow to reduce the systematic error coming from the application of general atmospheric profile which are not representative of the local conditions of the atmosphere. The presence of multiple-scattered photons not properly treated in the simulation chain is also a source of systematic uncertainties. The effect of the multiple-scattering process is to re-direct scattered photons, which are primarily suppressed from the solid angle of the detector, in the direction of the telescope focal surface leading to an increase of the detected signal. A proper treatment of the multiple-scattering processes in the simulation is needed to reduce this source of systematic effect. Finally, a big contribution to the systematic uncertainties will come from the inversion method eventually used to compute the atmospheric variables. For instance, one of the most common method used, the Klett inversion [20] has an associated systematic uncertainty of around 30 %.

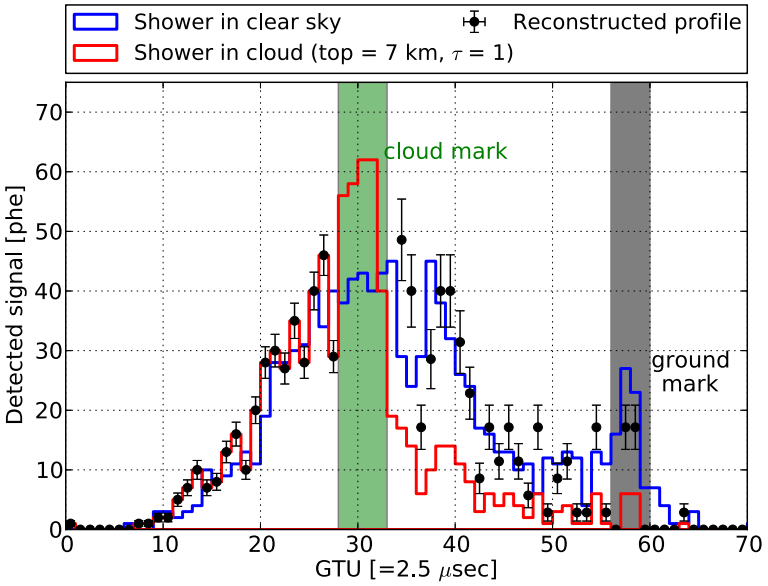

Fig. 6 Reconstructed time profile (*black points*) of 10^{20} eV EAS together with the clear atmosphere (*blue*) and cloud affected (*red*) profiles already shown in Fig. 4. Error bars are statistical only. The loss of information inside the cloud does not allow for a good reconstruction of the profile in that region. The ground mark (*gray band*) is almost entirely recovered by this procedure

5 Global atmospheric models

Analysis of both the IR camera and LIDAR data can be improved if the physical parameters of the atmosphere (temperature and pressure profiles, humidity, wind speed, etc.) in the monitored region are known [21]. Weather forecasting services across the world, such as NOAA's NCEP and NASA's GMAO in US or ECWMF in Europe, systematically collect all the available meteorological data, for example from weather stations, meteorological balloons, satellite and aircraft measurements, to use them as input data for the Global Atmospheric Models (GAM), which are computer generated models of atmospheric conditions at the entire Earth. The product of the model is an estimation of the state of the atmosphere, or state variables at any given point on a latitude-longitude grid and at different times. This calculation takes into account the real-time conditions of the atmosphere as a boundary condition for the global model. As a result, data products, e.g. temperature, pressure and humidity profiles, are available. In particular, some of them, such as GMAO/GEOS-5 (http://gmao.gsfc.nasa.gov/products/GEOS-5_FP_details.php), include information on the presence and altitude distribution of cloud and aerosol layers, which is directly relevant for JEM-EUSO data analysis.

Currently some efforts have been made by the collaboration to investigate the possibility of using data from the Global Data Assimilation System (GDAS) of NCEP (http://www.ncdc.noaa.gov/model-data/global-data-assimilation-system-gdas). The

GDAS provides an analysis every three hours and 3, 6, and 9-hour forecasts. GDAS data set contains several state variables as a function of the altitude in form of pressure levels from 1000 hPa (sea level) to 20 hPa ($\sim$ 26 km). Data are distributed in a latitude-longitude ($181° \times 360°$) grid of $1°$ spacing (http://ready.arl.noaa.gov/gdas1.php). GDAS data have been successfully incorporated in JEM-EUSO simulations of the air showers. The final goal is to incorporate GDAS data in the modelling of the atmosphere in the EAS reconstruction analysis and to create a database to be used in the analysis of the data of the LIDAR and IR camera in JEM-EUSO.

6 Conclusions

JEM-EUSO is a next-generation fluorescence telescope which will detect UHECR induced EAS from space. To reconstruct EAS profiles correctly, knowledge of the atmospheric condition at the location of the shower is mandatory. The Atmospheric Monitoring system of JEM-EUSO will comprise an IR camera, a LIDAR and global atmospheric model data to provide necessary information of the state of the atmosphere around the location of EAS events. The IR camera will provide the overall picture of the optically thick cloud cover within the JEM-EUSO FoV, while the LIDAR will give information about aerosol layers and clouds (altitude and optical depth), in particular optically thin clouds which are not detectable with the IR camera. Real-time atmospheric profiles from global models will be used as an input for the off-line analysis of LIDAR data, calibration of the IR camera and reconstruction of the EAS profile. The first step will be to select those events which are not affected by the presence of clouds and could be used as a "golden sample" for the UHECR analysis. In the following step, those events which are affected from the presence of clouds will be recovered using the information obtained from the analysis of the atmospheric data. Following the example presented in Section 4.2, the time profile of an observed event could be reconstructed using the knowledge on the cloud layers obtained from the LIDAR measurement.

Additional information on atmospheric conditions of some specific ground based sites would be provided by the Global Light System (GLS), namely flashes and tracks generated by a network of calibrated UV light sources on ground [22]. The GLS will comprise UV steerable laser and Xenon flashlamp stations which will be used to monitor and validate key parameters of the detector, such as trigger efficiency, the accuracy of intrinsic luminosity measurement and the pointing accuracy of a reconstructed event direction. JEM-EUSO will pass over a GLS station on average every 48 hours during moonless nights in clear atmospheric conditions. At the time of each GLS trigger the AM system will be activated, the IR Camera will acquire an IR image of the FoV and the LIDAR will shoot the GLS station. In these conditions the AM system could be used to cross check the atmospheric corrections derived from the GLS system. In addition, the GLS will provide an independent verification of some of the cloud free conditions in the JEM-EUSO FoV, allowing to reduce the systematic uncertainties.

Acknowledgments This work was partially supported by Basic Science Interdisciplinary Research Projects of RIKEN and JSPS KAKENHI Grant (22340063, 23340081, and 24244042), by the Italian Ministry of Foreign Affairs, General Direction for the Cultural Promotion and Cooperation, by the 'Helmholtz Alliance for Astroparticle Physics HAP' funded by the Initiative and Networking Fund of the Helmholtz Association, Germany, and by Slovak Academy of Sciences MVTS JEM-EUSO as well as VEGA grant agency project 2/0076/13. The Spanish Consortium involved in the JEM-EUSO Space Mission is funded by MICINN under projects AYA2009- 06037-E/ESP, AYA-ESP 2010-19082, AYA2011-29489-C03- 01, AYA2012-39115-C03-01, CSD2009-00064 (Consolider MULTIDARK) and by Comunidad de Madrid (CAM) under project S2009/ESP-1496.

References

1. Adams, J.H. Jr., et al.: (JEM-EUSO Collaboration). Astroparticle Phys. **44**, 76 (2013)
2. Picozza, P., Ebisuzaki, T., Santangelo, A.: For the JEM-EUSO Collaboration. The JEM-EUSO Mission. This issue
3. Shinozaki, K., Saez, G., Guzman, A.: For the JEM-EUSO Collaboration. JEM-EUSO observation in cloudy conditions. This issue
4. Sáez- Cano, G., et al.: For the JEM-EUSO collaboration. Observation of ultra-high energy cosmic rays in cloudy conditions by the JEM-EUSO space observatory. In: Proceedings of 32nd International Cosmic Ray Conference (ICRC), vol. 3, pp. 231. Beijing. (Preprint) arXiv:1204.5065 (2011)
5. Wada, S., et al.: For the JEM-EUSO collaborators. Potential of the atmospheric monitoring system of JEM-EUSO Mission. In: Proceedings 31st International Cosmic Ray Conference Lodz (2009)
6. Rodríguez Frías, M.D.: For the JEM-EUSO collaboration. The atmospheric monitoring system of the JEM-EUSO space mission. In: Proceedings International Symposium on Future Directions in UHECR Physics, CERN. EPJ Web of Conferences **53**, 10005 (2013)
7. Santangelo, A., Picozza, P., Ebisuzaki, T.: For the JEM-EUSO collaboration. Status of the JEM-EUSO mission. In: Proceedings of 33rd International Cosmic Ray Conference (ICRC). Rio de Janeiro. (Preprint) arXiv:1307.7071 (2013)
8. Neronov, A., Wada, S., Rodriguez Frias, M.D., et al.: Atmospheric monitoring system of JEM-EUSO. In: Proceedings of 32nd International Cosmic Ray Conference (ICRC), vol.6, pp. 332. Beijing. (Preprint) arXiv:1204.5065 (2011)
9. Garino, F., et al.: (JEM-EUSO Collaboration). Cloud coverage and its implications for cosmic ray observation from space. In: Proceedings of 32nd International Cosmic Ray Conference (ICRC). Beijing, ID0398 (2011)
10. Sáez Cano, G., et al.: Observation of ultra-high energy cosmic rays in cloudy conditions by the space-based JEM-EUSO observatory. J. Phys. Conf. Series **375**, 052010 (2012)
11. Sáez Cano, G., Shinozaki, K., del Peral, L., Bertaina, M., Rodriguez Frias, M.D.: Observation of extensive air showers in cloudy conditions by the JEM-EUSO space mission. In: Advances in Space Research: Special Issue, Centenary of the discover of the Cosmic Rays. In press (2013)
12. Morales de los Rós, J.A., et al.: The IR-camera of the JEM-EUSO space observatory. In: Proceedings of 32nd International Cosmic Ray Conference (ICRC), vol. 11, pp. 466. Beijing (2011)
13. Morales de los Rios, J.A., Joven, E., del Peral, L., Reyes, M., Licandro, J., Rodriguez Frias, M.D. (2013)
14. Rodríguez Frías, M.D., Briz, S.: For the JEM-EUSO Collaboration. The Infrared Camera onboard JEM-EUSO. This issue
15. Casolino, M., Kajino, F.: for the JEM-EUSO Collaboration. An Overview of the JEM-EUSO Instrument. This issue
16. Kawasaki, Y., et al.: (JEM-EUSO collaboration). The focal surface detector of the JEM-EUSO telescope. In: Proceedings of 32nd ICRC. Beijing, ID0472 (2011)
17. Dagoret, S., Barrillon, P., Jung, A. for the JEM-EUSO Collaboration, "The Photodetector Module of the JEM-EUSO mission", This issue
18. Berat, C., et al.: Full simulation of space-based extensive air showers detectors with ESAFs. Astropart. Phys. **33**(4), 221–247 (2010)

19. Toscano, S., et al.: (JEM-EUSO Collaboration). LIDAR treatment inside the ESAF simulation framework for the JEM-EUSO mission. In: Proceedings of 33nd ICRC. Rio De Janeiro. ID0530 (2013)
20. Klett, J.D.: Stable analytical inversion solution for processing Lidar returns. Appl. Opt. **20**, 211 (1981)
21. Keilhauer, B., Will, M.: For the Auger collaboration. Description of atmospheric conditions at the Pierre Auger observatory using meteorological measurements and models. Eur. Phys. J. Plus **127**, 96 (2012)
22. Gorodetzky, P., Christl, M., Haungs, A.: For the JEM-EUSO Collaboration. The Calibration Aspects of the JEM-EUSO Mission. This issue

The JEM-EUSO Collaboration

J.H. Adams Jr.[md], S. Ahmad[bb], J.-N. Albert[ba], D. Allard[bc], L. Anchordoqui[mf], V. Andreev[me], A. Anzalone[dh,dn], Y. Arai[ev], K. Asano[et], M. Ave Pernas[kc], P. Baragatti[do], P. Barrillon[ba], T. Batsch[hc], J. Bayer[cd], R. Bechini[dl], T. Belenguer[kb], R. Bellotti[da,db], K. Belov[me], A.A. Berlind[mh], M. Bertaina[dk,dl], P.L. Biermann[cb], S. Biktemerova[ia], C. Blaksley[bc], N. Blanc[la], J. Błęcki[hd], S. Blin-Bondil[bb], J. Blümer[cb], P. Bobik[ja], M. Bogomilov[aa], M. Bonamente[md], M.S. Briggs[md], S. Briz[kd], A. Bruno[da], F. Cafagna[da], D. Campana[df], J-N. Capdevielle[bc], R. Caruso[dc,dn], M. Casolino[ew,di], C. Cassardo[dk,dl], G. Castellini[dd], C. Catalano[bd], O. Catalano[dh,dn], A. Cellino[dk,dm], M. Chikawa[ed], M.J. Christl[mg], D. Cline[me], V. Connaughton[md], L. Conti[do], G. Cordero[ga], H.J. Crawford[ma], R. Cremonini[dl], S. Csorna[mh], S. Dagoret-Campagne[ba], A.J. de Castro[kd], C. De Donato[di], C. de la Taille[bb], C. De Santis[di,dj], L. del Peral[kc], A. Dell'Oro[dk,dm] N. De Simone[di], M. Di Martino[dk,dm], G. Distratis[cd], F. Dulucq[bb], M. Dupieux[bd], A. Ebersoldt[cb], T. Ebisuzaki[ew], R. Engel[cb], S. Falk[cb], K. Fang[mb], F. Fenu[cd], I. Fernández-Gómez[kd], S. Ferrarese[dk,dl], D. Finco[do], M. Flamini[do], C. Fornaro[do], A. Franceschi[de], J. Fujimoto[ev], M. Fukushima[eg], P. Galeotti[dk,dl], G. Garipov[ic], J. Geary[md], G. Gelmini[me], G. Giraudo[dk], M. Gonchar[ia], C. González Alvarado[kb], P. Gorodetzky[bc], F. Guarino[df,dg], A. Guzmán[cd], Y. Hachisu[ew], B. Harlov[ib], A. Haungs[cb], J. Hernández Carretero[kc], K. Higashide[er,ew], D. Ikeda[eg], H. Ikeda[ep], N. Inoue[er], S. Inoue[eg], A. Insolia[dc,dn], F. Isgrò[df,dp], Y. Itow[en], E. Joven[ke], E.G. Judd[ma], A. Jung[fb], F. Kajino[ei], T. Kajino[el], I. Kaneko[ew], Y. Karadzhov[aa], J. Karczmarczyk[hc], M. Karus[cb], K. Katahira[ew], K. Kawai[ew], Y. Kawasaki[ew], B. Keilhauer[cb], B.A. Khrenov[ic], Jeong-Sook Kim[fa], Soon-Wook Kim[fa], Sug-Whan Kim[fd], M. Kleifges[cb], P.A. Klimov[ic], D. Kolev[aa], I. Kreykenbohm[ca], K. Kudela[ja], Y. Kurihara[ev], A. Kusenko[me], E. Kuznetsov[md], M. Lacombe[bd], C. Lachaud[bc], J. Lee[fc], J. Licandro[ke], H. Lim[fc], F. López[kd], M.C. Maccarone[dh,dn], K. Mannheim[ce], D. Maravilla[ga], L. Marcelli[dj], A. Marini[de], O. Martinez[gc], G. Masciantonio[di,dj], K. Mase[ea], R. Matev[aa], G. Medina-Tanco[ga], T. Mernik[cd], H. Miyamoto[ba], Y. Miyazaki[ec], Y. Mizumoto[el], G. Modestino[de], A. Monaco[da,db], D. Monnier-Ragaigne[ba], J.A. Morales de los Ríos[ka,kc], C. Moretto[ba], V.S. Morozenko[ic], B. Mot[bd], T. Murakami[ef], M. Nagano[ec], M. Nagata[eh], S. Nagataki[ek], T. Nakamura[ej], T. Napolitano[de], D. Naumov[ia], R. Nava[ga], A. Neronov[lb], K. Nomoto[eu], T. Nonaka[eg], T. Ogawa[ew], S. Ogio[eo], H. Ohmori[ew], A.V. Olinto[mb], P. Orleański[hd], G. Osteria[df], M.I. Panasyuk[ic], E. Parizot[bc], I.H. Park[fc], H.W. Park[fc], B. Pastircak[ja], T. Patzak[bc], T. Paul[mf], C. Pennypacker[ma], S. Perez Cano[kc], T. Peter[lc], P. Picozza[di,dj,ew], T. Pierog[cb], L.W. Piotrowski[ew], S. Piraino[cd,dh], Z. Plebaniak[hc], A. Pollini[la], P. Prat[bc], G. Prévôt[bc], H. Prieto[kc], M. Putis[ja], P. Reardon[md], M. Reyes[ke], M. Ricci[de], I. Rodríguez[kd], M.D. Rodríguez Frías[kc], F. Ronga[de], M. Roth[cb], H. Rothkaehl[hd], G. Roudil[bd], I. Rusinov[aa], M. Rybczyński[ha], M.D. Sabau[kb], G. Sáez Cano[kc], H. Sagawa[eg], A. Saito[ej], N. Sakaki[cb], M. Sakata[ei], H. Salazar[gc], S. Sánchez[kd], A. Santangelo[cd], L. Santiago Crúz[ga], M. Sanz Palomino[kb], O. Saprykin[ib], F. Sarazin[mc], H. Sato[ei], M. Sato[es], T. Schanz[cd], H. Schieler[cb], V. Scotti[df,dg], A. Segreto[dh,dn], S. Selmane[bc], D. Semikoz[bc], M. Serra[ke], S. Sharakin[ic], T. Shibata[eq], H.M. Shimizu[em], K. Shinozaki[ew,cd], T. Shirahama[er], G. Siemieniec-Oziębło[hb], H.H. Silva López[ga], J. Sledd[mg], K. Słomińska[hd], A. Sobey[mg], T. Sugiyama[em], D. Supanitsky[ga], M. Suzuki[ep], B. Szabelska[hc], J. Szabelski[hc], F. Tajima[ee], N. Tajima[ew], T. Tajima[cc], Y. Takahashi[es], H. Takami[ev], M. Takeda[eg], Y. Takizawa[ew], C. Tenzer[cd], O. Tibolla[ce], L. Tkachev[ia], H. Tokuno[et], T. Tomida[ew], N. Tone[ew], S. Toscano[lb], F. Trillaud[ga], R. Tsenov[aa], Y. Tsunesada[et], K. Tsuno[ew], T. Tymieniecka[hc], Y. Uchihori[eb], M. Unger[cb], O. Vaduvescu[ke], J.F. Valdés-Galicia[ga], P. Vallania[dk,dm], L. Valore[df,dg], G. Vankova[aa], C. Vigorito[dk,dl], L. Villaseñor[gb], P. von Ballmoos[bd], S. Wada[ew], J. Watanabe[el], S. Watanabe[es], J. Watts Jr.[md], M. Weber[cb], T.J. Weiler[mh], T. Wibig[hc], L. Wiencke[mc], M. Wille[ca], J. Wilms[ca], Z. Włodarczyk[ha], T. Yamamoto[ei], Y. Yamamoto[ei], J. Yang[fb],

H. Yano[ep], I.V. Yashin[ic], D. Yonetoku[ef], K. Yoshida[ei], S. Yoshida[ea], R. Young[mg], M.Yu. Zotov[ic], A. Zuccaro Marchi[ew]

[aa] St. Kliment Ohridski University of Sofia, Bulgaria
[ba] LAL, Univ Paris-Sud, CNRS/IN2P3, Orsay, France
[bb] Omega, Ecole Polytechnique, CNRS/IN2P3, Palaiseau, France
[bc] APC, Univ Paris Diderot, CNRS/IN2P3, CEA/Irfu, Obs. de Paris, Sorbonne Paris Cité, France
[bd] IRAP, Université de Toulouse, CNRS, Toulouse, France
[ca] ECAP, University of Erlangen-Nuremberg, Germany
[cb] Karlsruhe Institute of Technology (KIT), Germany
[cc] Ludwig Maximilian University, Munich, Germany
[cd] Inst. for Astronomy and Astrophysics, Kepler Center, University of Tübingen, Germany
[ce] Institut für Theoretische Physik und Astrophysik, University of Würzburg, Germany
[da] Istituto Nazionale di Fisica Nucleare - Sezione di Bari, Italy
[db] Universita' degli Studi di Bari Aldo Moro and INFN - Sezione di Bari, Italy
[dc] Dipartimento di Fisica e Astronomia - Universita' di Catania, Italy
[dd] Consiglio Nazionale delle Ricerche (CNR) - Ist. di Fisica Applicata Nello Carrara, Firenze, Italy
[de] Istituto Nazionale di Fisica Nucleare - Laboratori Nazionali di Frascati, Italy
[df] Istituto Nazionale di Fisica Nucleare - Sezione di Napoli, Italy
[dg] Universita' di Napoli Federico II - Dipartimento di Scienze Fisiche, Italy
[dh] INAF - Istituto di Astrofisica Spaziale e Fisica Cosmica di Palermo, Italy
[di] Istituto Nazionale di Fisica Nucleare - Sezione di Roma Tor Vergata, Italy
[dj] Universita' di Roma Tor Vergata - Dipartimento di Fisica, Roma, Italy
[dk] Istituto Nazionale di Fisica Nucleare - Sezione di Torino, Italy
[dl] Dipartimento di Fisica, Universita' di Torino, Italy
[dm] Osservatorio Astrofisico di Torino, Istituto Nazionale di Astrofisica, Italy
[dn] Istituto Nazionale di Fisica Nucleare - Sezione di Catania, Italy
[do] UTIU, Dipartimento di Ingegneria, Rome, Italy
[dp] DIETI, Universita' degli Studi di Napoli Federico II, Napoli, Italy
[ea] Chiba University, Chiba, Japan
[eb] National Institute of Radiological Sciences, Chiba, Japan
[ec] Fukui University of Technology, Fukui, Japan
[ed] Kinki University, Higashi-Osaka, Japan
[ee] Hiroshima University, Hiroshima, Japan
[ef] Kanazawa University, Kanazawa, Japan
[eg] Institute for Cosmic Ray Research, University of Tokyo, Kashiwa, Japan
[eh] Kobe University, Kobe, Japan
[ei] Konan University, Kobe, Japan
[ej] Kyoto University, Kyoto, Japan
[ek] Yukawa Institute, Kyoto University, Kyoto, Japan
[el] National Astronomical Observatory, Mitaka, Japan
[em] Nagoya University, Nagoya, Japan
[en] Solar-Terrestrial Environment Laboratory, Nagoya University, Nagoya, Japan
[eo] Graduate School of Science, Osaka City University, Japan
[ep] Institute of Space and Astronautical Science/JAXA, Sagamihara, Japan
[eq] Aoyama Gakuin University, Sagamihara, Japan
[er] Saitama University, Saitama, Japan
[es] Hokkaido University, Sapporo, Japan
[et] Interactive Research Center of Science, Tokyo Institute of Technology, Tokyo, Japan
[eu] University of Tokyo, Tokyo, Japan
[ev] High Energy Accelerator Research Organization (KEK), Tsukuba, Japan
[ew] RIKEN, Wako, Japan
[fa] Korea Astronomy and Space Science Institute (KASI), Daejeon, Republic of Korea
[fb] Ewha Womans University, Seoul, Republic of Korea
[fc] Sungkyunkwan University, Seoul, Republic of Korea
[fd] Center for Galaxy Evolution Research, Yonsei University, Seoul, Republic of Korea
[ga] Universidad Nacional Autónoma de México (UNAM), Mexico

[gb] Universidad Michoacana de San Nicolas de Hidalgo (UMSNH), Morelia, Mexico
[gc] Benemérita Universidad Autónoma de Puebla (BUAP), Mexico
[ha] Jan Kochanowski University, Institute of Physics, Kielce, Poland
[hb] Jagiellonian University, Astronomical Observatory, Krakow, Poland
[hc] National Centre for Nuclear Research, Lodz, Poland
[hd] Space Research Centre of the Polish Academy of Sciences (CBK), Warsaw, Poland
[ia] Joint Institute for Nuclear Research, Dubna, Russia
[ib] Central Research Institute of Machine Building, TsNIIMash, Korolev, Russia
[ic] Skobeltsyn Institute of Nuclear Physics, Lomonosov Moscow State University, Russia
[ja] Institute of Experimental Physics, Kosice, Slovakia
[ka] Consejo Superior de Investigaciones Científicas (CSIC), Madrid, Spain
[kb] Instituto Nacional de Técnica Aeroespacial (INTA), Madrid, Spain
[kc] Universidad de Alcalá (UAH), Madrid, Spain
[kd] Universidad Carlos III de Madrid, Spain
[ke] Instituto de Astrofísica de Canarias (IAC), Tenerife, Spain
[la] Swiss Center for Electronics and Microtechnology (CSEM), Neuchâtel, Switzerland
[lb] ISDC Data Centre for Astrophysics, Versoix, Switzerland
[lc] Institute for Atmospheric and Climate Science, ETH Zürich, Switzerland
[ma] Space Science Laboratory, University of California, Berkeley, USA
[mb] University of Chicago, USA
[mc] Colorado School of Mines, Golden, USA
[md] University of Alabama in Huntsville, Huntsville, USA
[me] University of California (UCLA), Los Angeles, USA
[mf] University of Wisconsin-Milwaukee, Milwaukee, USA
[mg] NASA - Marshall Space Flight Center, USA
[mh] Vanderbilt University, Nashville, USA